

Dear Dr. Tian,

We would like to thank you and the two reviewers for your reviews of our manuscript “Emergent stationarity in Yellow River sediment transport and the underlying shift of dominance: from streamflow to vegetation”. We appreciate these insightful inputs that have helped to improve the quality of this manuscript. In response to the comments, we have made corresponding revisions. Our response to each comment is listed below in blue with the specific line numbers of the changes we have made. Again, we appreciate the time and inputs from you and the reviewers.

Best regards,
Sheng Ye,
Qihua Ran,
Xudong Fu,
Chunhong Hu,
Guangqian Wang,
Gary Parker,
Xiuxiu Chen,
Siwei Zhang

Anonymous Referee #1

Accepted as is.

Thank you!

Anonymous Referee #2

Substantial improvement has been made in the revision. However, there are still several minor problems to be answered, which are listed below:

We appreciate the reviewer's comments which help improve our manuscript significantly. We have also made the suggested changes this time. Our response to each comment is listed below in blue with the changes in manuscript, we also include the specific line numbers of the changes we have made.

(1) The notations such as Q_a and Q_m are suggested to be added in the labels of figures to avoid confusion between them.

We have added the Q_a and Q_m notation to the labels of Figure 1 and Figure S4. Thank you for pointing this out.

(2) Since most of the results were analyzed among different gauges, that is to say the correlations detected are spatial rather than temporal correlations, the authors may introduce this information in the caption of figures and the corresponding text.

We agree with the reviewer that it helps avoid the potential confusion with the introduction of this information. We have added this in the caption of Figure 1 and 2 as well as the corresponding text (please see lines 141 -142, 145, 151, and 189). We hope the reviewer finds this sufficient.

(3) In Line 94-95 of the revised manuscript, what's the difference between NDVI and LTDR? Why use "instead of"?

NDVI is a vegetation index derived from remote sensing data; while LTDR and GIMMS are data projects storing different products including NDVI. The reason we used the NDVI from LTDR instead of the NDVI from GIMMS is that NDVI from LTDR provides better estimation of the vegetation in the YRB. We are sorry about this confusion due to our writing. We have now revised it (please see line 94), hopefully it is clear now. Thank you!

1 Emergent stationarity in Yellow River sediment transport and the
2 underlying shift of dominance: from streamflow to vegetation

3 Sheng Ye¹, Qihua Ran^{1*}, Xudong Fu², Chunhong Hu³, Guangqian Wang², Gary
4 Parker⁴, Xiuxiu Chen¹, Siwei Zhang¹

5

6 ¹ Institute of Hydrology and Water Resources, Department of Hydraulic Engineering,
7 Zhejiang University, Hangzhou 310058, China

8 ² State Key Laboratory of Hydro-science and Engineering, Tsinghua University,
9 Beijing 100084, China

10 ³ State Key Laboratory of Simulation and Regulation of Water Cycle in River Basin,
11 Institute of Water Resources and Hydropower Research, Beijing 100048, China

12 ⁴ Department of Civil & Environmental Engineering and Department of Geology,
13 University of Illinois at Urbana-Champaign, Urbana, Illinois 61801, USA

14 * Corresponding author: Qihua Ran (ranqihua@zju.edu.cn)

15

16 Submitted to: *Hydrology and Earth System Sciences*

17

18 | ~~Nov-Jan~~ 10³th 2019~~8~~

19

20 **Abstract**

21 Soil erosion and sediment transport play important roles in terrestrial landscape
22 evolution and biogeochemical cycles of nutrients and contaminants. Although
23 discharge is considered to be a controlling factor in sediment transport, its correlation
24 with sediment concentration varies across the Yellow River Basin (YRB) and is not
25 fully understood. This paper provides analysis from gauges across the YRB covering
26 a range of climate, topographic characteristics and degree of human intervention. Our
27 results show that discharge control on sediment transport is dampened at gauges with
28 large mean annual discharge, where sediment concentration becomes more and more
29 stable. This emergent stationarity can be attributed to vegetation resistance. Our
30 analysis shows that sediment concentration follows a bell shape with vegetation index
31 (normalized difference vegetation index, NDVI) at annual scale despite heterogeneity
32 in climate and landscape. We obtain the counterintuitive result that as mean annual
33 discharge increases, the dominant control on sediment transport shifts from
34 streamflow erosion to vegetation retardation in the YRB.

35 **Keywords:** Yellow River Basin, sediment, stationarity, vegetation, bell-shape

36

37 1. Introduction

38 Watershed sediment transport, from hillslope to channel and subsequently the coast, is
39 crucial to erosion management, flood control, river delta development, and the
40 quantification of global biogeochemical cycles of materials such as organic
41 phosphorus, iron, and aluminum (Martin and Meybeck, 1979; [He et al., 2014](#)). During
42 the 20th century, human activities have significantly modified the landscape, leading
43 to a reduction in sediment yield and coastal retreat worldwide (Walling and Fang,
44 2003; Syvitski et al., 2005). Known for its severe sediment problems, the Yellow
45 River (YR) has been a hotspot for studies on soil erosion and sediment transport for
46 decades. Since the 1950s, the annual sediment yield has reduced by 80% because of
47 check dam construction and ecosystem restoration such as the Grain-for-Green project,
48 motivating discussion on the necessity for further expansion of re-vegetation schemes
49 (Chen et al., 2015).

50 Most studies on the physical mechanisms of soil erosion and sediment transport were
51 conducted in relatively small sub-catchments (Collins et al., 2004; Ran et al., 2012).
52 In order to interpret the patterns discovered at basin scale, then, it is essential to
53 understand the scaling effects of soil erosion and sediment transport. Specifically,
54 would the mechanisms identified at small scale also prevail at basin scale? If not,
55 what factors influence upscaling (Mutema et al., 2015; Song et al., 2016). However,
56 existing studies on the scaling effects of sediment transport are rather limited, and
57 show no significant spatial coherence in the scaling of sediment transport (Le
58 Bissonnais et al., 1998; Deasy et al., 2011; Song et al., 2016). Due to the great

59 heterogeneity in the YRB, scaling patterns could be different even within one tributary.
60 Taking the Wuding River as example, event mean concentration could decrease
61 downstream after the initial increase in one sub-catchment (Zheng et al., 2011) or
62 keep rising until reaching a plateau in another sub-catchment nearby (Fang et al.,
63 2008). Not only the sediment concentration, but also its correlation with discharge
64 varies across the YRB. Although discharge is considered as one of the controlling
65 factors in sediment transport, how its influence upscales remains to be fully
66 understood. Therefore it is necessary to expand our findings concerning sediment
67 transport from single tributaries to larger scales, especially incorporating diverse
68 climate, environmental and anthropogenic characteristics, so that we can derive an
69 understanding applicable to the whole YRB. In this paper, we collected observations
70 across the Yellow River Basin (YRB) to quantify changes in sediment concentration
71 in the recent decades (Rustomji et al., 2008; Miao et al., 2011; Wang et al., 2016). By
72 analyzing data from gauges across the YRB (Figure S1), we attempt to understand:
73 how the correlation between sediment concentration and discharge varies across
74 spatial and temporal scales; what are the dominant factors influencing sediment
75 transport in the YRB; and how their contributions vary from place to place.

76 **2. Data and methodology**

77 We collected daily discharge and sediment concentration data from 123 hydrology
78 gauges within our study area: the YRB above Sanmenxia station, the major
79 hydropower station on the YR. From these we selected 68 gauges spanning a range of

80 climate conditions and physiographic areas, from the gauge at the most upstream end
81 of the main stem to the gauges above Tongguan, which just 100km upstream of
82 Sanmengxia Dam (Figure S1). These gauges were selected for at least 15-year (1971
83 – 1986) continuous daily discharge and sediment concentration records between 1951
84 and 1986. For comparison and further examination of our hypothesis, we also extract
85 the annual discharge and concentration data between 2000 and 2012 for seven gauges
86 located at the outlet of the major tributaries from the Yellow River Sediment Bulletin
87 (Figure S1 green stars).

88 The vegetation data used in this study corresponds to the normalized difference
89 vegetation index (NDVI), which is an index calculated from remote sensing
90 measurements to indicate the density of plant growth (Running et al., 2004). The
91 NDVI data was downloaded from NASA's Land Long Term Data Record (LTDR)
92 project, which provides daily NDVI observations globally at a spatial resolution of
93 0.05°. Instead of the NDVI obtained from Global Inventory Modeling and Mapping
94 Studies (GIMMS), [the NDVI from LTDR project](#) is chosen for its better estimation in
95 the YRB (Sun et al., 2015). The daily NDVI data from 44 gauges located on the eight
96 major tributaries were collected and extracted according to the drainage area of the
97 study gauges from 1982 to 2012 (Figure S1 green stars). The gauges on the main stem
98 of YR were not used as the water and sediment condition there is more likely
99 controlled by the major dams along the main stem rather than the hillslope
100 characteristics. Annual maximum NDVI values were used to represent the highest
101 vegetation productivity. The precipitation and leaf area index (LAI) data of the US

102 catchments used for comparison are assembled from the first author's previous work
103 (Ye et al., 2015).

104 To examine the coupling between discharge and sediment concentration at various
105 temporal scales, wavelet coherence analysis was applied to the daily discharge (m^3/s)
106 and sediment concentration (kg/m^3) data following Grinsted et al (2004). Wavelet
107 transforms decompose time series into time and frequency and can be used to analyze
108 different parts of the time series by varying the window size. They have been applied
109 to geophysical records for the understanding of variability at temporal scales. To
110 examine the co-variation between discharge and concentration in the time frequency
111 domain, we used a wavelet coherence defined as (Grinsted et al 2004)

$$112 \quad R^2(s) = \frac{|S(s^{-1}W^{XY}(s))|^2}{S(s^{-1}|W^X(s)|^2)*S(s^{-1}|W^Y(s)|^2)} \quad (1)$$

113 where S is a smoothing operator, W^{XY} is cross wavelet transform of time series X and
114 Y representing the common power between the two series, s refers to scale and W^X
115 and W^Y are the continuous wavelet transforms of time series X and Y respectively.
116 The wavelet coherence can be considered as a correlation coefficient of the two time
117 series in the time frequency domain. The region of cone of influence (COI) was
118 delineated in the wavelet coherence images to avoid reduction in confidence caused
119 by edge effects. Localized wavelets were also averaged through temporal scales to
120 obtain global wavelet coherence (Guan et al., 2011). More detailed explanation about
121 wavelet coherence analysis can be found in Grinsted et al (2004).

122 The annual discharge (Q_a) and the sediment yield (L_a) were aggregated from daily to
123 further examine their correlation:

$$124 \quad Q_a = (\sum_{i=1}^n (Q_i * 3600 * 24)) / Ad * 1000 \quad (2)$$

$$125 \quad L_a = (\sum_{i=1}^n (Q_i * C_i * 3600 * 24)) \quad (3)$$

126 where Q_i (m^3/s) and C_i (kg/m^3) are the daily discharge and sediment concentration, Ad
127 is the drainage area (km^2) of each gauge, n is the number of days in each year. This
128 analysis is applied only at annual scale since this is when the coupling from wavelet
129 coherence analysis is the strongest (the one with the largest wavelet coherence). The
130 annual mean concentration (C_a) was calculated as:

$$131 \quad C_a = L_a / (Q_a * Ad / 1000) \quad (4)$$

132 The long-term mean annual discharge (Q_m) and the long-term mean annual
133 concentration (C_m) was also calculated by averaging for the period of 1951 to 1986.
134 Note that both the parameters Q_a and Q_m used here are area-specific discharges
135 (mm/yr). For each gauge, a linear regression was fit to describe the correlation
136 between annual discharge (Q_a) and annual mean concentration (C_a). The slope of this
137 linear regression (α_{QC}) is used to describe the rate of change in sediment
138 concentration with changing discharge at annual scale.

139 3. The emergent stationarity in sediment concentration

140 We applied wavelet coherence analysis to daily discharge and sediment concentration
141 data at 68 study gauges across the YRB (Figure S2, S3). The results show that, across
142 the gauges, the coupling between discharge and concentration (Q-C) declines with

143 mean annual discharge (Q_m) at all three temporal scales (Figure 1a). That is, as Q_m
144 increases, the influence of streamflow on sediment transport becomes weaker and
145 weaker across the gauges, both at intra-annual and within-year scales.

146 This fading impact of streamflow as it increases can be further quantified in terms of a
147 linear regression between discharge (Q_a) and mean sediment concentration (C_a) at
148 annual scale, when the coupling between discharge and concentration (Q-C) is the
149 strongest (Figure S4). As can be seen from Figure 1b, though annual mean
150 concentration is positively correlated with annual discharge at most gauges, the slope
151 in the Q-C regression (α_{QC}) declines exponentially with Q_m across the gauges (p -value
152 < 0.0001). The larger Q_m is, the less sensitive sediment concentration responds to
153 variation in annual discharge. For example, gauges with α_{QC} less than 0.1 are the ones
154 with Q_m larger than 60mm/yr. When Q_m is larger than 100mm/yr, the variation in
155 sediment concentration is less than 1% of that in streamflow ($\alpha_{QC} < 0.01$), and thus
156 sediment concentration can be approximated as invariant to changing discharge. Most
157 of these gauges locate on the main stem or near the outlets of tributaries. This
158 increased independence between sediment concentration and discharge may be
159 attributed to the heterogeneity in these relatively large catchments.

160 This emergent stationarity explains the linear correlation between area-specific
161 sediment yield and runoff depth reported in a small sub-watershed in a hilly area of
162 the Loess Plateau (Zheng et al., 2013). Considering the sediment concentration to be
163 constant, the variation in yield is solely dominated by streamflow, resulting in the

164 observed linear discharge-yield relationship. Similar stationarity in sediment
165 concentration has also been found in arid watersheds in Arizona (Gao et al., 2013), US
166 where the sediment concentration becomes homogeneous among watersheds when
167 their drainage area is larger than 0.01 km^2 . The difference in threshold for the
168 emergence of approximately discharge-invariant concentration between the YRB and
169 watersheds in Arizona, US is probably due to the differences in catchment
170 characteristics, i.e. vegetation type and coverage, terrestrial structure, soil properties,
171 etc.

172 Our analysis shows that mean annual discharge (Q_m) is a better indicator of the
173 correlation between water and sediment transport than drainage area, although the last
174 parameter has been used traditionally. Despite the heterogeneity, both the coupling
175 between Q-C and the concentration sensitivity to variation in streamflow decreases
176 with Q_m . A closer inspection reveals useful insights. At gauges with smaller values of
177 Q_m , discharge is the dominant factor in sediment transport: an increment in annual
178 discharge is amplified in the increment of sediment concentration ($\alpha_{QC} > 1$) (i.e.
179 Gauge 808, 812 in Figure S4). However, as Q_m increases, variation in streamflow is
180 more weakly reflected in variation in sediment concentration, even though annual
181 mean concentration still correlates with annual discharge, (i.e. Gauge 806 in Figure
182 S4). As Q_m continues to increase, sediment concentration becomes almost invariant to
183 discharge, suggesting that the dominant factor of sediment transport has shifted from
184 the discharge to something else.

185 **4. The vegetation impact: a bell shape**

186 To further explore the potential cause of this emergent stationarity, we analyzed the
187 vegetation data (NDVI) from 44 of the gauges locating on eight major tributaries of
188 the YR (Figure S1). Our analysis shows that this declining sensitivity in concentration
189 at annual scale (α_{QC}) is negatively related to vegetation impact across the gauges
190 (Figure 2).

191 For gauges with limited vegetation establishment in their drainage area, the variation
192 in discharge is amplified in sediment transport ($\alpha_{QC}>1$). The larger the discharge is at
193 specific year, the more sediment is eroded and mobilized per cubic meter. This
194 dominance of discharge is weakened when vegetation density and coverage increase.
195 Despite the larger sediment carrying capacity of larger discharge, sediment
196 concentration is reduced, probably due to the protection vegetation offers against
197 erosion. As maximum NDVI increase, sediment concentration becomes less and less
198 coupled with discharge at annual scale. When the vegetation density is sufficiently
199 high, sediment concentration is nearly stable in spite of the variation in discharge,
200 since the dense vegetation coverage protects soil from erosion and traps sediment.
201 That is, the emergent stationarity in sediment concentration corresponding to the
202 variation in discharge at gauges with large Q_m can be attributed to the dampened
203 dominance of discharge due to the increasing impact of vegetation retardation.

204 To further confirm the vegetation impact on sediment transport, we derived the plot
205 between maximum NDVI and mean concentration at annual scale in Figure 3a. As we

206 can see, the annual mean sediment concentration follows a bell-shaped correlation
207 with vegetation establishment, with a peak concentration at a value of maximum
208 NDVI of around 0.36. On the falling limb of this bell curve, as NDVI increases, both
209 sediment concentration and α_{QC} decrease consistently. That is, both the value of
210 concentration and its sensitivity to streamflow variation declines with increasing
211 vegetation index on the falling limb. To confirm this impact of vegetation resistance,
212 we also examined the relationship between sediment concentration and other
213 catchment characteristic like dominant soil type. No significant correlation was
214 observed as vegetation did. Although there could still be other factors not considered
215 here contributed to the decline in sediment concentration, it is undoubted that
216 vegetation is one of the most influential factors of sediment reduction and can be used
217 as a good indicator of the soil erosion and sediment transport in the YRB.

218 On the rising limb, however, both the value of concentration and its sensitivity to
219 streamflow variation increases with increasing vegetation index. Most gauges have
220 values α_{QC} larger than one, except one gauge with an extremely small maximum
221 value of NDVI. For these gauges, on the rising limb, vegetal cover is still low in an
222 absolute sense despite increasing NDVI. Sediment concentration is mainly dominated
223 by discharge: fluctuations in streamflow are amplified in concentration ($\alpha_{QC}>1$). The
224 only gauge with a value of α_{QC} smaller than one is gauge HanJiaMao (HJM) at the
225 Wuding River. Although the annual precipitation and discharge at HJM is similar to
226 other gauges along the Wuding River, the annual mean sediment concentration is
227 much smaller. This is because of the extremely high baseflow contribution in

228 discharge at HJM, which is around 90%, thanks to very intensive check-dam
229 construction there (Dong and Chang, 2014). Since sediment in the YRB is mostly
230 transported during large flow events during the summer, smaller flow events are not
231 capable of transporting significant sediment loads at HJM.

232 In general, we can conclude that sediment transport is mainly dominated by discharge
233 when the vegetation index is low. With increasing NDVI, the impact of vegetation
234 grows slowly at first, and accelerates after the maximum NDVI exceeds 0.36.
235 Eventually, the effect of NDVI takes over the dominance of streamflow, and
236 attenuates the variation in sediment concentration (Figure 4). The nonlinear impact of
237 vegetation in regard to resistance of sediment to erosion is consistent with previous
238 findings (Rogers and Schumm, 1991; Collins et al., 2004; Temmerman et al., 2005;
239 Corenblit et al., 2009). When the vegetation index level is low, its resistance to soil
240 erosion develops slowly as vegetation grows and expands (Rogers and Schumm,
241 1991), and capability of vegetation to trap sediment is reduced when submerged by
242 flood (Temmerman et al., 2005) or overland flow. Therefore, for catchments with
243 limited vegetation establishment, the coverage of vegetation is insufficient to trap
244 sediment, nor is the vegetation able to protrude from the water level during the
245 extreme flow events that transport most of the sediment. Sediment transport in these
246 catchments is usually dominated by discharge. As NDVI increases, vegetation
247 becomes much more capable as an agent of erosion protection and sediment settling
248 (Jordanova and James 2003; Corenblit et al., 2009). With the compensation from
249 vegetation retardation, sediment and discharge become more and more decoupled as

250 discharge increases, so that concentration is nearly invariant to increasing discharge.
251 The transition point in maximum NDVI (around 0.36) is where the increment in
252 vegetation reduction balances with the incremental increase in water erosion. When
253 the capability of vegetation retardation catches up with streamflow erosion, the net
254 soil loss becomes negligible, a condition commonly observed in well-vegetated
255 regions.

256 **5. Validation of the bell shape across time and space**

257 Since 1999, a large-scale ecosystem restoration project, the ‘Grain-for-Green’ project
258 was launched in the YRB for soil conservation (Lv et al., 2012). It has substantially
259 improved vegetation coverage after a decade of implementation (Sun et al., 2015). To
260 validate our hypothesis gain from the early 1980s, we applied similar analysis to the
261 annual flow and sediment data as well as daily NDVI data at seven gauges located at
262 the outlets of major tributaries from 2008 to 2012 (Figure S1 green stars). This is the
263 period subsequent to the initiation of the ‘Grain-for-Green’ project. We have excluded
264 the years right after the implementation of the ‘Grain-for-Green’ project, when there
265 was an initial drastic change in vegetation coverage and sediment erosion and
266 transport processes.

267 As we can see from Figure 3b, there is significant increase in maximum NDVI for all
268 seven catchments, and considerable reduction in mean sediment concentration. This
269 improvement is consistent with the previous report that the ‘Grain-for-Green’ project
270 has made a remarkable achievement in regard to soil conservation in the YRB (Chen

271 et al., 2015). Comparison of the relationship between sediment concentration and
272 maximum NDVI in the early 1980s and around 2010 shows that the bell shape
273 relationship sustains even after drastic and significant anthropogenic alteration of the
274 land use and land cover across the whole YRB. Although the vegetation coverage has
275 improved significantly at all seven comparison gauges due to the ecosystem
276 restoration policy, and thereby effectively moderated sediment erosion; the bell shape
277 relationship between maximum NDVI and mean concentration sustains.

278 Similar bell shape relationship was also found for the multi-year mean annual
279 precipitation and sediment yield observed in the United States (Langbein and Schumm,
280 1958). The data used in the analysis of Langbein and Schumm (1958) was collected in
281 the 1950s from more humid and vegetated catchments with limited human
282 intervention, on the opposite of the YRB. Yet similar bell shape was still observed
283 between sediment yield and precipitation. Given the limited anthropogenic activities
284 in these catchments, vegetation growth is probably to correlate with annual
285 precipitation due to its adaption to climate, as in other US catchments (Figure S6).
286 Thus it is likely that a bell shape correlation between vegetation and sediment yield
287 would be found at these US catchments as well. This suggests that the bell shape
288 correlation between vegetation and sediment concentration is not only observed in the
289 YRB with intensive human intervention, but could also be valid outside it. More
290 analyses are needed to test this relationship in other catchments outside the YRB for
291 its universality.

292 **6. Implications and conclusion**

293 Our analysis shows that across the YRB, both the correlation between Q and C and
294 the magnitude of sediment response to the variation in streamflow decreases with Q_m .
295 When Q_m is sufficiently large (i.e. > 60 mm/yr), sediment concentration reaches a
296 stationary (constant) state at annual scale. The emergent stationarity at gauges with
297 large Q_m is related to the shift of dominance from discharge to vegetation. Because of
298 the slow development of vegetation resistance with increasing discharge for small
299 discharges, discharge dominates the soil erosion and sediment transport process until
300 the maximum NDVI exceeds a threshold (0.36 for this study), at which the parameter
301 governing concentration transits from streamflow erosion to vegetation retardation.

302 Our findings of the emergent stationarity in sediment concentration and the shift of
303 the dominant mechanism governing the Q-C relation have important implications for
304 water and sediment management at watershed scale. Our study indicates that for the
305 gauges with relatively large discharge, the annual mean concentration can be
306 approximated as a constant over a large range of discharges. Thus the estimation of
307 sediment yield can be simply inferred from a simulation of streamflow. First order
308 estimates of sediment yield for scientific or engineering purposes can be obtained by
309 multiplying the estimated discharge by a constant sediment concentration estimated
310 based upon the vegetation index. The correlation between vegetation and sediment
311 concentration will also be useful for the design of the ongoing ecosystem restoration
312 program known as the 'Grain-for-Green' project. The bell-shaped correlation between

313 maximum NDVI and sediment concentration provides a quantitative way to estimate
314 the potential change in sediment concentration associated with proposed ecosystem
315 restoration planning schemes at and near each tributary. This can help guide land use
316 management so as to allocate the sediment contribution from each of the upstream
317 tributaries in a way that maintains the balance between erosion and deposition in the
318 lower YR.

319 It is important to collect more data from the current decade (i.e. after the substantial
320 ecosystem restoration) to further validate our findings in regard to emergent
321 stationarity and vegetation impact at more gauges in the YRB. It will be helpful if we
322 could examine our findings in other watersheds worldwide with different climate and
323 vegetation types. Although humid regions are usually considered as well-vegetated,
324 study shows that there could still be erosion issues in these areas due to topographic
325 gradient, precipitation intensity, and soil properties, etc. (Holz et al., 2015). Analysis
326 with more field measurements could also help explain the threshold discharge of the
327 emergent stationarity. Numerical simulations as well as long-term measurements on
328 the soil properties are also needed to further explain the physical mechanism of
329 vegetation retardation: how it develops its impact on soil erosion and sediment
330 transport by changing soil properties and other topographic characteristics during its
331 growth and spread.

332 **Acknowledgements**

333 This research was financially supported by the National Key Research and
334 Development Program of China (2016YFC0402404, 2016YFC0402406) and the

335 National Natural Science Foundation of China (51509218, 51379184, 51679209). All
336 the data used in this study were downloaded from websites indicated in Materials and
337 Methods section in Supplementary. The authors thank Dr. Jinren Ni for insightful
338 discussion.

339 **References**

340 Chen, Y. P., K. B. Wang, Y. S. Lin, W. Y. Shi, Y. Song, and X. H. He (2015),
341 Balancing green and grain trade, *Nat Geosci* 8: 739-741.

342 Collins, D. B. G., R. L. Bras, and G. E. Tucker (2004), Modeling the effects of
343 vegetation-erosion coupling on landscape evolution, *J Geophys Res* 109: 121 –
344 141.

345 Corenblit, D., J. Steiger, A. M. Gurnell, E. Tabacchi, and L. Roques (2009), Control of
346 sediment dynamics by vegetation as a key function driving biogeomorphic
347 succession within fluvial corridors. *Earth Surf Process Landforms* 34: 1790–1810.

348 Deasy ,C., S. A. Baxendale, A. L. Heathwaite, G. Ridall, R. Hodgkinson, and R. E.
349 Brazier (2011), Advancing understanding of runoff and sediment transfers in
350 agricultural catchments through simultaneous observations across scales, *Earth*
351 *Surf Process Landforms* 36: 1749–1760.

352 Dong, J and L. Chang (2014), Analysis of runoff characteristic change and influence
353 for Hailiutu River, *J Water Resour. & Water Eng* 25: 143 – 147.

354 Fang, H. Y., Q. G. Cai, H. Chen, and Q. Y. Li (2008), Temporal changes in suspended
355 sediment transport in a gullied loess basin: The lower Chabagou Creek on the
356 Loess Plateau in China. *Earth Surf Process Landforms* 33: 1977–1992.

357 Gao, P., M. A. Nearing, and M. Commons (2013), Suspended sediment transport at

358 the instantaneous and event time scales in semiarid watersheds of southeastern
359 Arizona, USA. *Water Resour Res* 49: 6857–6870.

360 Grinsted, A., S. Jevrejeva, and J. Moore (2004), Application of the cross wavelet
361 transform and wavelet coherence to geophysical time series. *Nonlinear Proc*
362 *Geoph* 11: 561–566.

363 Guan, K., S. E. Thompson, C. J. Harman, N. B. Basu, P. S. C. Rao, M. Sivapalan, A. I.
364 Packman, and P. K. Kalita (2011), Spatiotemporal scaling of hydrological and
365 agrochemical export dynamics in a tile-drained Midwestern watershed. *Water*
366 *Resour Res* 47: 1290 – 1300.

367 [He, Z., H. Weng, H. Ho, Q. Ran, M. Mao \(2014\), Soil erosion and pollutant transport](#)
368 [during rainfall-runoff processes. *Water Resour.*, 41\(5\), 604 – 611.](#)

369 Holz, D. J., K. W. J. Williard, P. J. Edwards, J. E. Schoonover (2015), Soil erosion in
370 humid regions: a review. *J Contemp Water Res Educ* 154: 48-59.

371 Jordanova, A. A., and C. S. James (2003), Experimental Study of Bed Load Transport
372 through Emergent Vegetation. *J Hydraul Eng* 129: 474-478.

373 Langbein, W. B., and S. A. Schumm (1958), Yield of sediment in relation to mean
374 annual precipitation, *Eos Trans. AGU*, 39(6), 1076-1084.

375 Le Bissonnais, Y., H. Benkhadra, V. Chaplot, D. Fox, D. King, and J. Daroussin
376 (1998), Crusting, runoff and sheet erosion on silty loamy soils at various scales
377 and upscaling from m² to small catchments. *Soil Tillage Res* 46: 69–80.

378 Lv, Y., B. Fu, X. Feng, Y. Zeng, Y. Liu, R. Chang, G. Sun, and B. Wu (2012), A
379 policy-driven large scale ecological restoration: quantifying ecosystem services

380 changes in the Loess Plateau of China. *PloS One*, 7 (2), e31782.

381 Martin, J. M. and M. Meybeck (1979), Elemental mass-balance of material carried by
382 major world rivers. *Mar Chem* 7: 173 – 206.

383 Miao, C. Y., J. R. Ni, A. G. L. Borthwick, and L. Yang (2011), A preliminary estimate
384 of human and natural contributions to the changes in water discharge and
385 sediment load in the Yellow River. *Global Planet Change* 76: 196–205.

386 Mutema, M., V. Chaplot, G. Jewitt, P. Chivenge, and G. Bloschl (2015), Annual
387 water, sediment, nutrient, and organic carbon fluxes in river basins: A global
388 meta-analysis as a function of scale. *Water Resour Res* 51: 8949– 8972.

389 Ran, Q., D. Su, P. Li, and Z. He (2012), Experimental study of the impact of rainfall
390 characteristics on runoff generation and soil erosion. *J Hydrol* 424 – 425: 99 –
391 111.

392 Rogers, R. D., and S. A. Schumm (1991), The effect of sparse vegetative cover on
393 erosion and sediment yield. *J Hydrol* 123: 19–24.

394 Running, S. W., F. A. Heinsch, M. Zhao, M. Reeves, H. Hashimoto, and R. R. Nemani
395 (2004), A continuous satellite-derived measure of global ter- restrial primary
396 production, *Bioscience*, 54(6), 547–560, doi:10.1641/
397 0006-3568(2004)054[0547:ACSMOG]2.0.CO;2.

398 Rustomji, P., X. P. Zhang, P. B. Hairsine, L. Zhang, and J. Zhao (2008), River
399 sediment load and concentration responses to changes in hydrology and catchment
400 management in the Loess Plateau of China. *Water Resour Res* 44: 148 - 152.

401 Song, C., G. Wang, X. Sun, R. Chang, and T. Mao (2016), Control factors and scale

402 analysis of annual river water, sediments and carbon transport in China. *Sci Rep* 6:
403 25963.

404 Sun, W., X. Song, X. Mu, P. Gao, F. Wang, and G. Zhao (2015), Spatiotemporal
405 vegetation cover variations associated with climate change and ecological
406 restoration in the Loess Plateau. *Agr Forest Meteorol* 209-210: 87–99.

407 Syvitski, J. P. M., C. J. Vorosmarty, A. J. Kettner, and P. Green (2005), Impact of
408 humans on the flux of terrestrial sediment to the global coastal ocean. *Science* 308:
409 376–380.

410 Temmerman, S., T. J. Bouma, G. Govers, Z. B. Wang, M. B. De Vries, and P. M. J.
411 Herman (2005), Impact of vegetation on flow routing and sedimentation patterns:
412 Three-dimensional modeling for a tidal marsh. *J Geophys Res* 110: 308 – 324.

413 Walling, D. E. and D. Fang (2003), Recent trends in the suspended sediment loads of
414 the world's rivers. *Global Planet Change* 39: 111 – 126.

415 Wang, S., B. Fu, S. Piao, Y. Lv, C. Philippe, X. Feng, and Y. Wang (2016), Reduced
416 sediment transport in the Yellow River due to anthropogenic changes. *Nat Geosci*
417 9: 38-41.

418 Ye, S., H.-Y. Li, S. Li, L. R. Leung, Y. Demissie, Q. Ran, and G. Blöschl (2015),
419 Vegetation regulation on streamflow intra-annual variability through adaption to
420 climate variations, *Geophys. Res. Lett.*, 42, 10,307–10,315, doi:10.1002/
421 2015GL066396.

422 Zheng, M. G., F. Qin, L. Y. Sun, D. L. Qi, and Q. G. Cai (2011), Spatial scale effects
423 on sediment concentration in runoff during flood events for hilly areas of the

424 Loess Plateau, China. *Earth Surf Process Landforms* 36: 1499–1509.

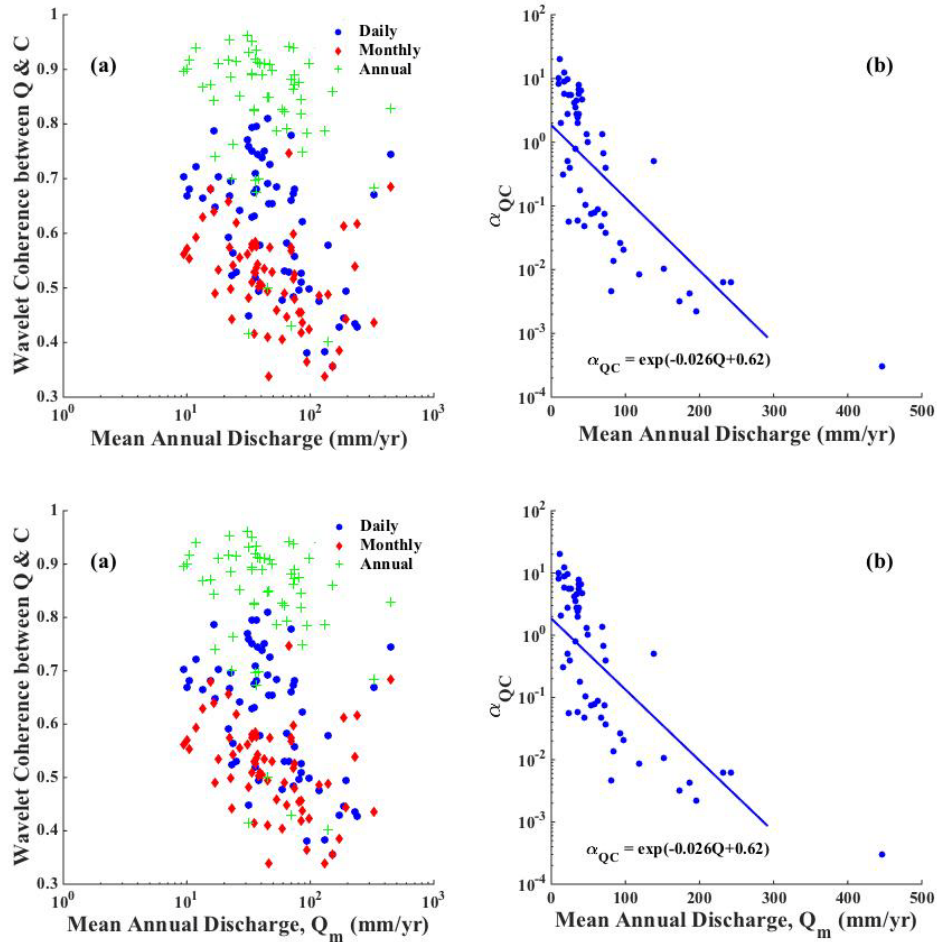
425 Zheng, M. G., F. Qin, J. S. Yang, and Q. G. Cai (2013), The spatio-temporal

426 invariability of sediment concentration and the flow–sediment relationship for

427 hilly areas of the Chinese Loess Plateau. *Catena* 109: 164–176.

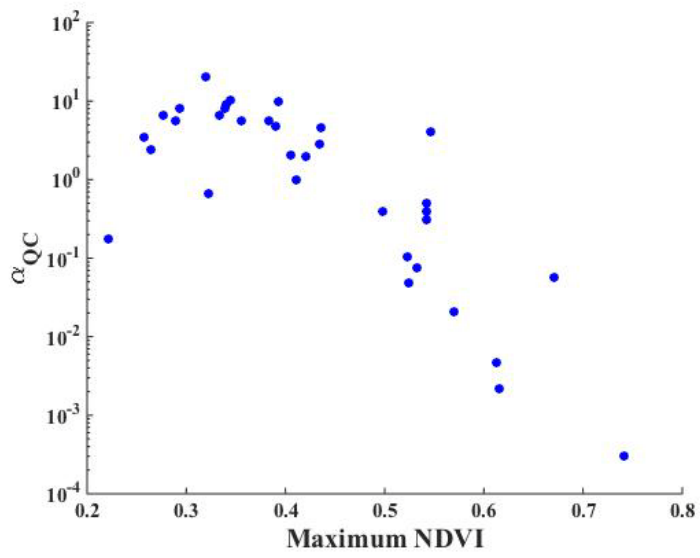
428

429 **Figure 1:** Scatter plots between long-term mean annual discharge (Q_m) and (a)
 430 wavelet Q - C coherence at daily, monthly and annual scales from the 68 study gauges,
 431 (b) slope of the discharge- sediment concentration regression (α_{QC}) at annual scale
 432 from the 68 study gauges, $R^2 = 0.55$ and p -value < 0.0001 .
 433



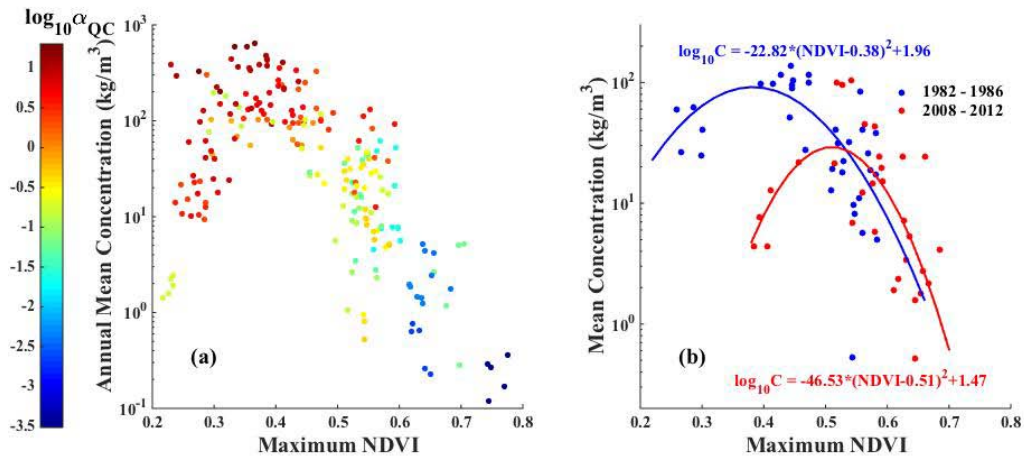
434
 435
 436

437 **Figure 2:** Scatter plots between the maximum NDVI and slope in the Q-C regression
438 at annual scale (α_{QC}) from the 44 study gauges.



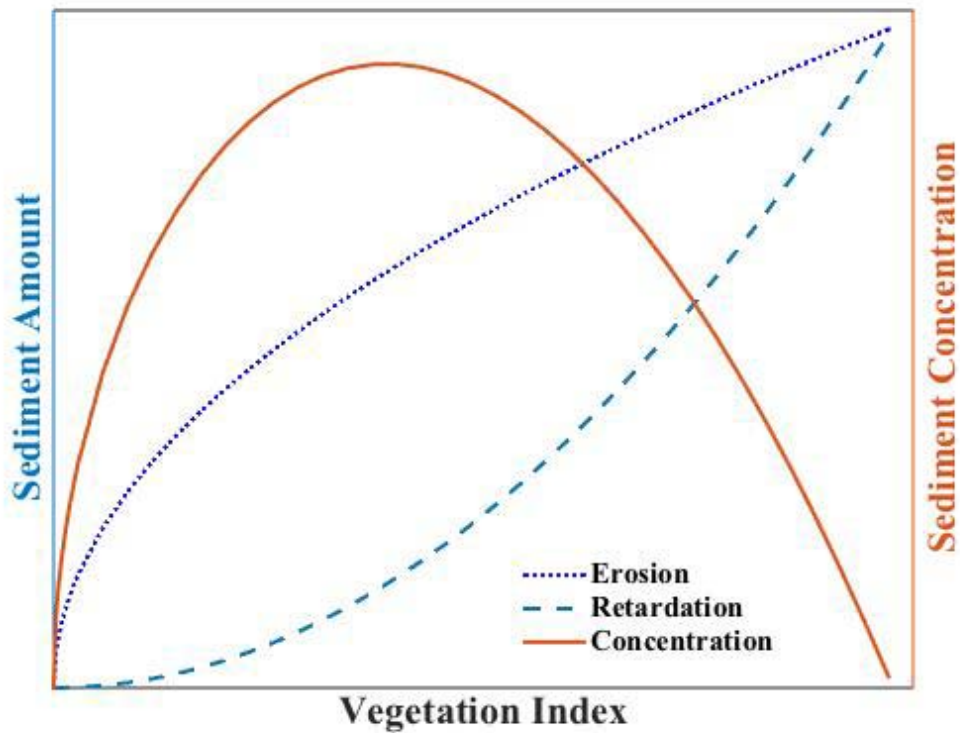
439

440 **Figure 3.** Scatter plot of annual mean concentration and maximum NDVI: (a) at 44
 441 study gauges between 1982 and 1986, where the dots are color-coded by the slope in
 442 the Q-C regression (α_{QC}) at each gauge; and (b) at 7 gauges with both data from the
 443 years 1982 – 1986 (blue dots) and the years 2008 – 2012 (red dots). The R^2 for the
 444 two fit is 0.6 and 0.44 respectively with p -value < 0.001 for both of them.



445

446 **Figure 4.** Illustration of the correlation between vegetation and sediment erosion,
447 retardation and the resulting sediment concentration in the YRB. Since vegetation
448 usually increases with discharge, with the rise in discharge, sediment eroded and
449 delivered by streamflow increases rapidly, while the retardation from vegetation is
450 limited at the beginning and increases fast afterwards. This non-synchronous impact on
451 sediment transport leads to the bell shape correlation between sediment concentration
452 and vegetation.



453

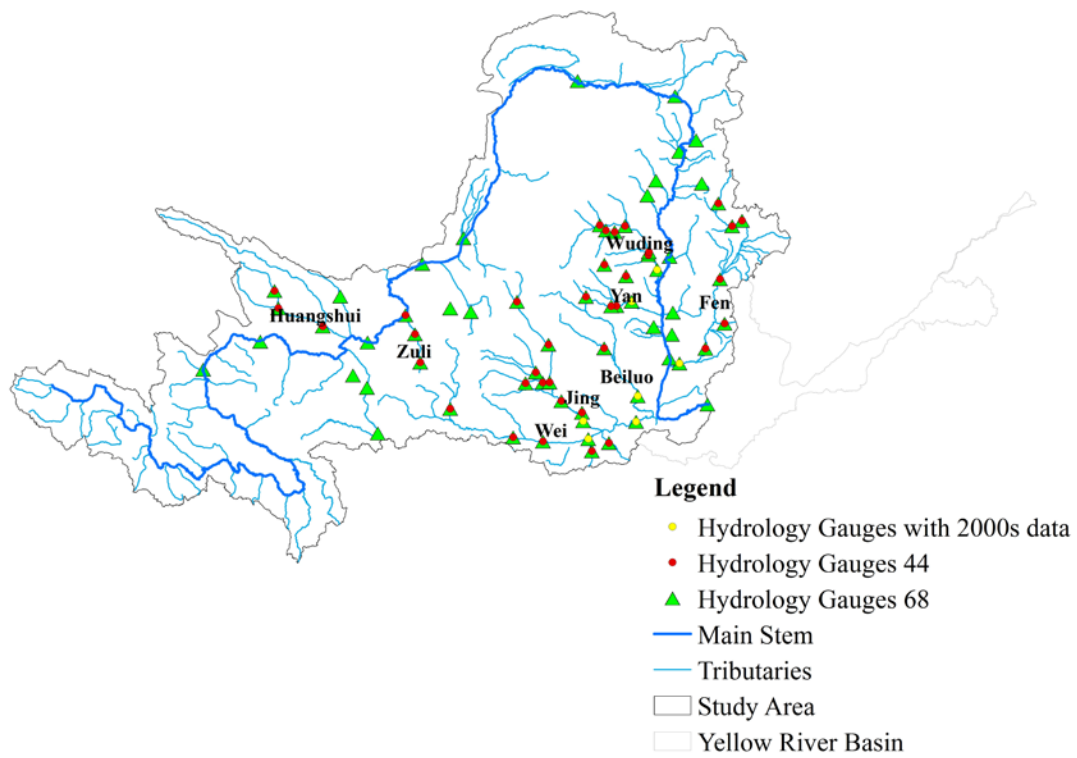
454

455

456

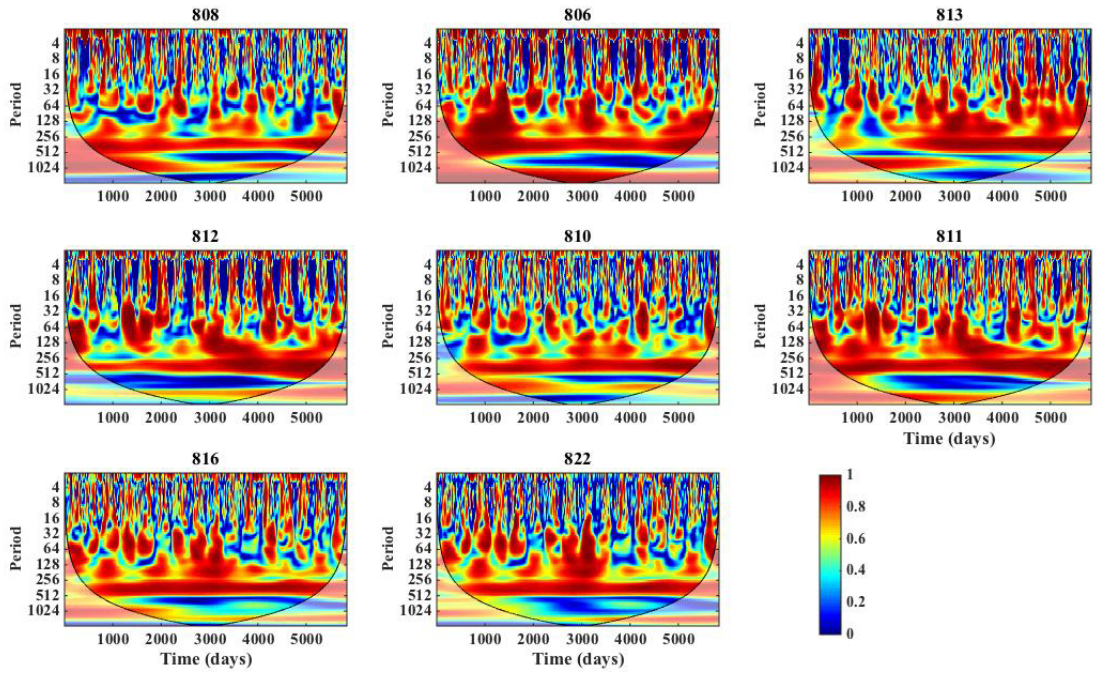
Supplementary

457 **Figure S1:** Spatial distribution of hydrology gauges used in this study. The green
458 triangles correspond to 68 gauges with discharge and sediment concentration data, the
459 red circles correspond to 44 selected gauges with NDVI data, and the yellow circles
460 are the ones with annual discharge and sediment data for the years 2000 – 2012.



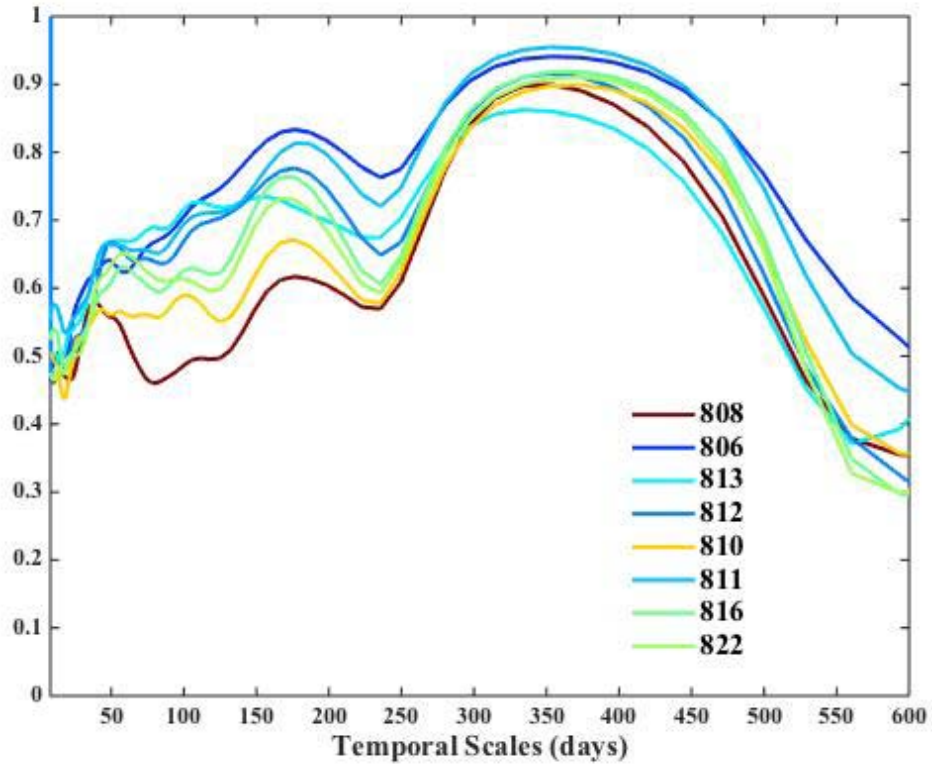
461

462 **Figure S2:** Wavelet coherence plots of the coupling between standardized discharge
463 and concentration, using the Jing River as an example. The labels correspond to the
464 gauge IDs. The shaded area is the cone of influence (COI) of edge effects.



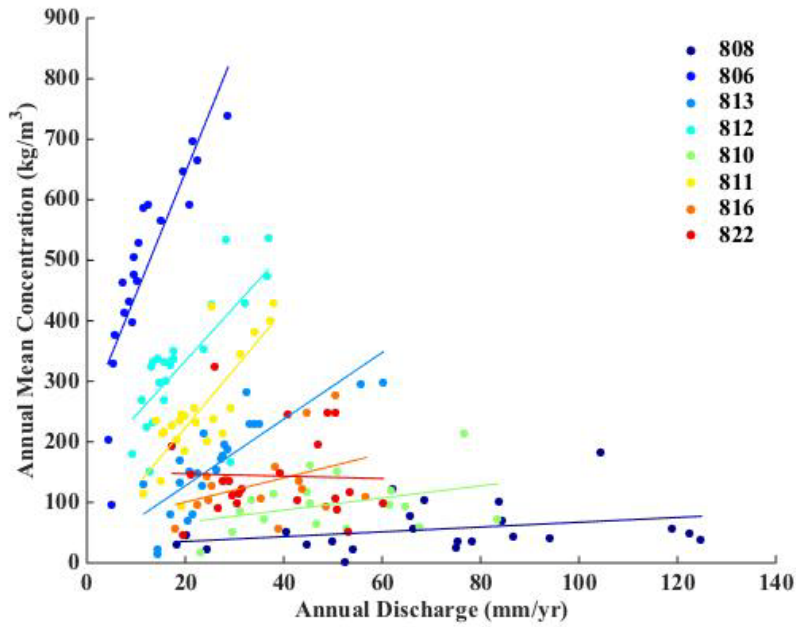
465

466 **Figure S3:** Averaged wavelet coherence plot, using the Jing River as an example. The
467 lines are colored according to long-term mean annual discharge (mm/yr), from blue to
468 brown as discharge increases.

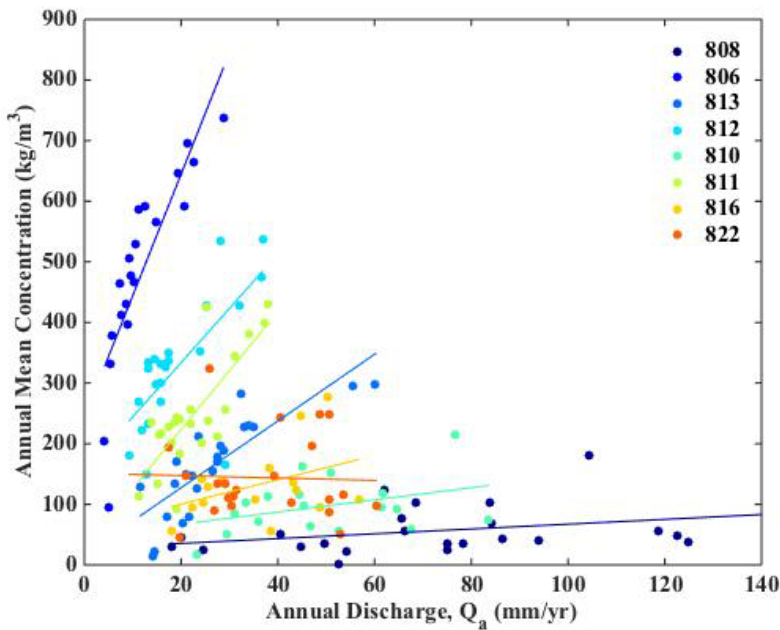


469
470

471 **Figure S4:** Scatter plot of the annual discharge and annual mean concentration from
472 1951 to 1986, as well as the result of linear regression between discharge and
473 concentration, using the gauges along the Jing River as an example.

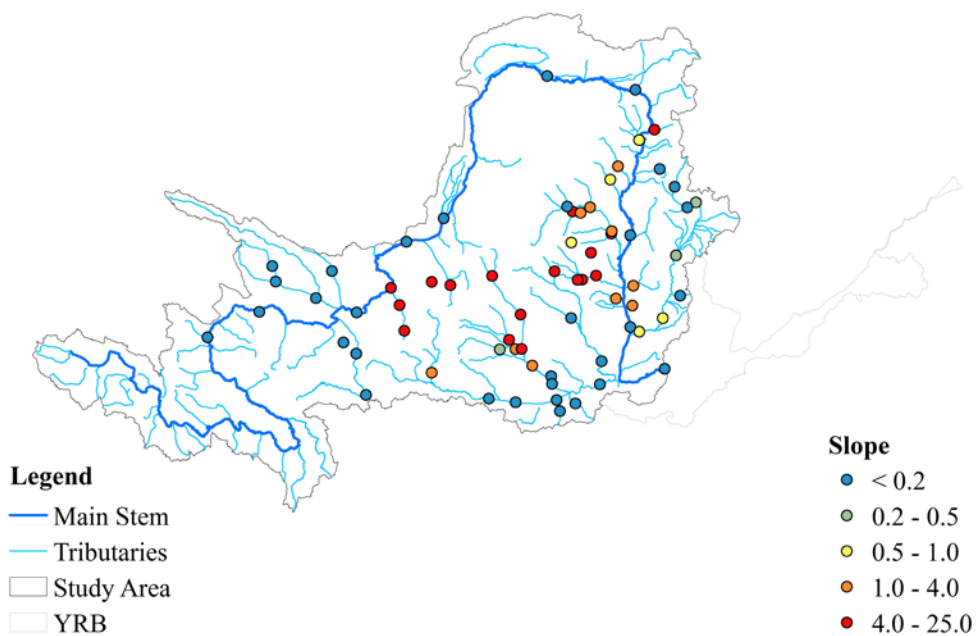


474



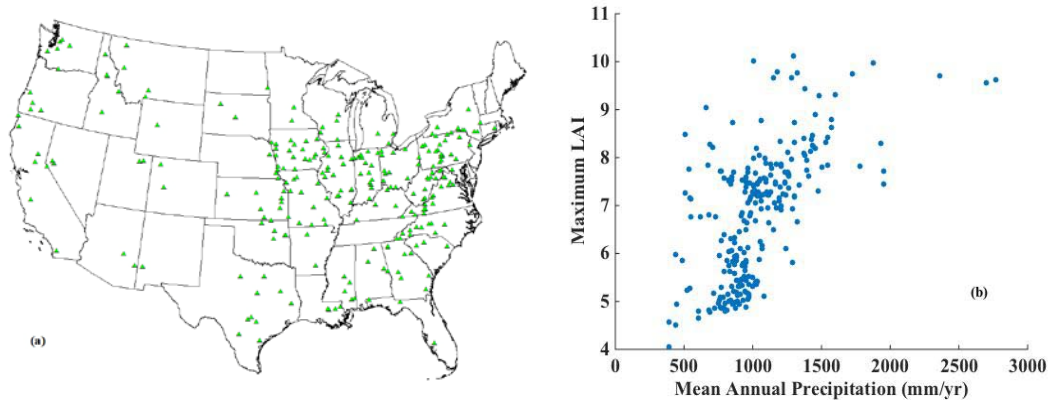
475

476 **Figure S5:** Spatial distribution of the slope of the Q-C regressions (α_{QC}).



477

478 **Figure S6.** a) Spatial distribution of the MOPEX catchments; b) scatter plot of mean
479 annual precipitation and annual maximum LAI for the MOPEX catchments.



480